Research Article | Vol. 26, No. 23 | 12 Nov 2018 | OPTICS EXPRESS 30420
Optics EXPRESS

Simultaneous acquisition of complex transmittance and birefringence with two counter-rotating, circularly polarized THz pulses

YOICHI KAWADA,[1,2,*] KATSUMASA YOSHIOKA,[2] YUSUKE ARASHIDA,[2] IKUFUMI KATAYAMA,[2] JUN TAKEDA,[2] AND HIRONORI TAKAHASHI[1]

[1]*Central Research Laboratory, Hamamatsu Photonics K.K., 5000 Hirakuchi, Hamakita, Hamamatsu City, Shizuoka 434-8601, Japan*
[2]*Department of Physics, Graduate School of Engineering, Yokohama National University, Yokohama 240-8501, Japan*
[*]*kawada401@crl.hpk.co.jp*

Abstract: Here we demonstrate simultaneous measurements of the complex transmittance and birefringence using left- and right-handed circularly polarized terahertz (THz) pulses. We change the polarization of the THz pulses periodically by modulating the polarization of the pump pulses directed onto a ZnTe (111) crystal, and we convert linear to circular polarization using a broadband THz quarter-wave retarder. By integrating the alternating-emission system with the polarization-sensitive terahertz time-domain spectrometer, we are able to obtain the electric-field vector of the transmitted terahertz pulses for both the left- and right-handed circular polarizations. Utilizing this technique, we are able to measure simultaneously the frequency-dependent complex refractive indices (real and imaginary parts) and the orientations of the slow and fast axes of birefringent materials, a quartz disc and a barium borate crystal, in a single temporal sweep.

1. Introduction

Measuring the polarization dependence of the optical constants is very important for THz-sensing technologies, because THz waves carry in-depth information about material properties such as anisotropy, chirality, and magnetism. Applications include ellipsometry to characterize the optical properties of bulk and thin-film materials [1], circular dichroism spectroscopy to distinguish left- and right-handed molecules [2], and polarization-resolved spectroscopy to image the elastic strain induced in a material [3]. It is also indispensable for the fundamental sciences, as it enables us to determine macroscopic quantum states of a material, such as electromagnons [4], the photo-Hall effect [5], and the strong light-matter coupling in Landau polaritons [6]. The recent observation of the Bloch–Siegert shift in Landau polaritons provides a striking example of polarization-resolved THz spectroscopy [6], in which the dependence of the transmittance on the polarization state of the incident THz pulses was measured using polarization-sensitive (PS) THz time-domain spectrometry (TDS).

Although PS-THz-TDS has been utilized for decades, it is still challenging to characterize precisely all the optical constants of a material, which describe completely its response to incident light with an arbitrary polarization state. To obtain a full characterization of these properties, we need to measure two orthogonal components of the transmitted THz electric field for two incident THz waves with orthogonal polarizations. Furthermore, to avoid the influence of temporal fluctuations in the laser power and temporal variations of the sample state, we need to acquire the entire set of measurements simultaneously and rapidly. Recently, the simultaneous detection of two orthogonal components of the THz electric field has been demonstrated by utilizing zinc blende crystals [7–9] and multi-contact photoconductive

#345301 https://doi.org/10.1364/OE.26.030420
Journal © 2018 Received 10 Sep 2018; revised 18 Oct 2018; accepted 18 Oct 2018; published 5 Nov 2018

Optics EXPRESS

antennas [10,11]. To characterize the optical properties of anisotropic materials, however, more than two temporal sweeps are still required, because there are eight independent optical constants for a material without depolarization [12]. However, only four variables (the amplitude and phase of the two orthogonal components) can be obtained from one polarization state of one incident THz pulse. Even for non-magnetic materials, there are still five independent constants, and a single scan is not sufficient to achieve full characterization.

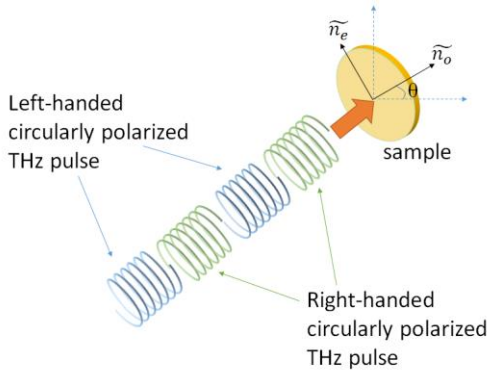

Fig. 1. Concept and overview of the measurement of a birefringent material by alternating emissions of two-polarization-state THz pulses.

In the present work, we demonstrate a novel technique for obtaining the temporal vector waveforms of right-handed and left-handed circularly polarized (RCP and LCP) THz pulses using only a single temporal sweep (see Fig. 1). We controlled the polarization state of the THz pulses by using a Pockels cell to change periodically the polarization state of the femtosecond (fs) laser pulse used to generate the terahertz pulse. By integrating the alternating-emission system with the PS-THz-TDS system, we were able to measure two orthogonal electric fields for each incident circularly polarized pulse. We thus acquired four independent electric-field components (i.e., eight variables) at once.

As a first demonstration, we have utilized this technique to measure the optical constants of two typical birefringent materials: a quartz disc and a barium borate (BBO) crystal. Using the circularly polarized THz pulses, we were able to probe both the slow and fast axes for arbitrary sample orientations. Since the method we propose here is capable of measuring the complex refractive index (real and imaginary parts) along two orthogonal axes (the slow and fast axes) together with the sample orientation, it can be applied to various birefringent materials, such as organic [13] and inorganic crystals [14,15], stretched elastomers and polymers [3,16], fiber-reinforced plastics [17,18], metamaterials exhibiting artificial anisotropy [19], and biomedical molecules [20]. In Sec. 2.1, we describe the method we used to generate THz pulses alternately with two orthogonal polarization states. In Sec. 2.2, we show how we detected the vector THz waveforms, and in Sec. 2.3 we describe how we integrated alternating emission and simultaneous measurements of RCP and LCP THz pulses.. In Sec. 3, we show how to determine the full set of optical parameters for anisotropic materials.

Optics EXPRESS

2. Simultaneous measurement of vector waveforms for THz pulses with two orthogonal polarizations

2.1 Alternate emission of THz pulses with two orthogonal polarizations

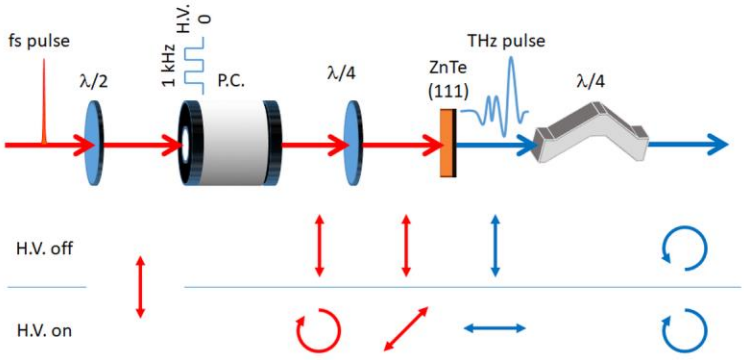

Fig. 2. Polarization state at each optical component of the alternating-emission system with the high voltage (H.V.) off and on.

Here we explain the procedure we used to obtain alternating emissions of RCP and LCP THz pulses, referring to Fig. 2. The pump pulses are linearly polarized fs-laser pulses [Micra, with the compact pulse compressor (CPC) option, from Coherent Inc., with an average power of 500 mW, a pulse width of 60 fs, and a repetition rate of 80 MHz]. A half-wave plate adjusts the polarization angle of a linearly polarized pump pulse to 45 degrees from the orientation of the Pockels cell. The Pockels cell is an electro-optical device that works as a transient wave plate when a high voltage (H.V., typically several kV) is applied. We pre-chirped the fs-laser pulse with the CPC to avoid pulse-stretching due to transmission through the Pockels cell (KD*P, length = 25 mm). We applied a quarter-wave voltage for 800-nm light to the Pockels cell at a repetition frequency of 1 kHz, and the pump pulse was converted to circularly polarized light when the H.V. was applied. Next, we positioned a quarter-wave plate so that its orientation was inclined 45 degrees to that of the Pockels cell. Without the H.V., the polarization angle of the pump pulse and the angle of the fast (or slow) axis of the quarter-wave plate were the same, so the polarization angle of the pump pulse did not change. In contrast, with the H.V. on, the circularly polarized pump pulse was converted again to a linearly polarized pulse, but the polarization angle was rotated by 45 degrees from the initial polarization angle. The pump pulses were directed onto a 1-mm-thick ZnTe (111) crystal, which converted them into THz pulses. The magnitude of the THz electric field emitted from the ZnTe (111) crystal is independent of the polarization angle of the pump pulse, while the emitted polarization angle changes according to the relation $\theta_{pump} = -2\theta_{THz}$, where θ_{pump} and θ_{THz} are the polarization angles of the pump pulses and THz pulses, respectively [21]. In this step, linearly polarized THz pulses with orthogonal polarization angles were emitted alternately. To change a linearly polarized THz pulse to a circularly polarized THz pulse without changing the optical path, we used an achromatic-prism quarter-wave retarder that covers a wide range of frequencies up to 4.5 THz [22]. We positioned the prismatic quarter-wave retarder so that its main axis was at an intermediate angle between the polarization angles of the alternately emitted THz pulses. As a result, RCP and LCP THz pulses were emitted alternately.

2.2 Vector detection of THz electric fields

In this section, we first explain the detection of the vector electric-field waveforms using our PS-THz-TDS.

Optics EXPRESS

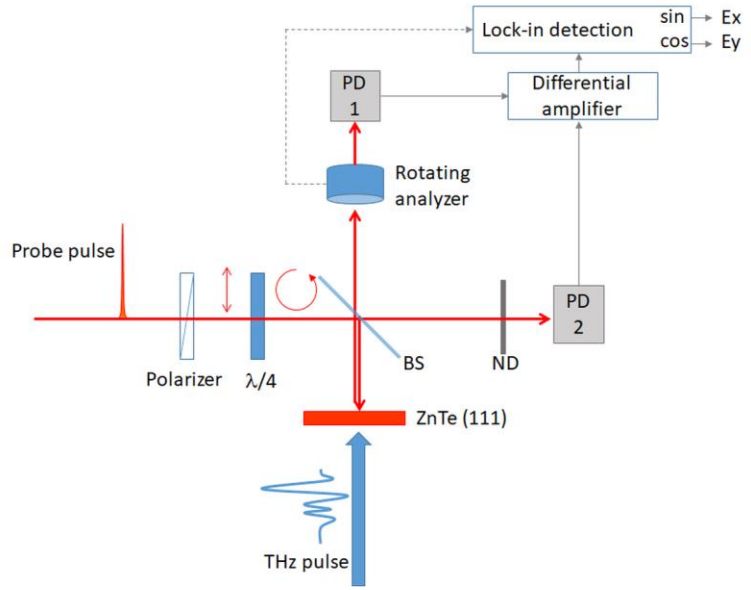

Fig. 3. Schematic diagram of our PS-THz-TDS.

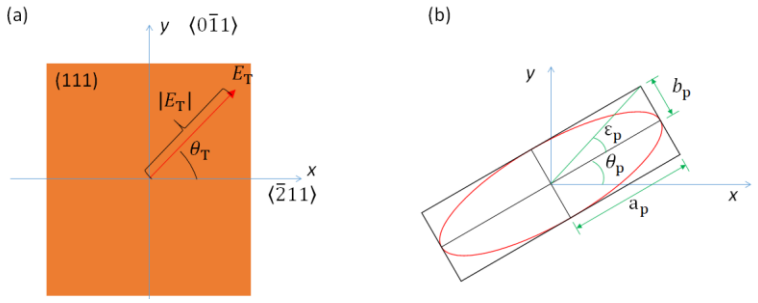

Fig. 4. Definition of (a) the THz electric-field amplitude (E_T) and the polarization direction (θ_T) at the ZnTe (111) crystal, and (b) the ellipticity angle (ε_p) and azimuth angle (θ_p) of the probe pulse.

Figure 3 shows a schematic diagram of our PS-THz-TDS. As probe pulses, we used 800 nm fs-laser pulses, which we converted into circularly polarized pulses by using a quarter-wave plate. We split the probe pulse into two pulses, one of which we used as a reference pulse to compensate for fluctuations in the laser power. We directed the circularly polarized probe pulses and the THz pulse onto a 1-mm-thick ZnTe (111) crystal and probed the THz electric field [8,23]. We used the following relations between the states of the THz pulse and the probe pulse, which we derived from equations in [24] (see Appendix 1):

$$\sin A_c |E_T| = \cos 2\varepsilon_p, \tag{1}$$

and

$$\theta_T = \frac{\pi}{2} - 2\theta_p, \tag{2}$$

where $|E_T|$ and θ_T are, respectively, the absolute value of the amplitude and the orientation of the THz electric field, as illustrated in Fig. 4(a); ε_p and θ_p are the ellipticity angle and the azimuthal angle of the probe pulse, as defined in Fig. 4(b); and A_c is a proportionality constant between the electric-field strength and the ellipticity angle, which is determined by the

Optics EXPRESS

thickness and nonlinear susceptibility of the electro-optical (EO) crystal (ZnTe). As can be seen from Eqs. (1) and (2), the absolute value of the THz electric-field amplitude and the ellipticity angle of the probe pulse have a one-to-one relationship, and the orientation of the THz electric field and the azimuthal angle of the probe pulse also have a one-to-one relationship. This shows that if the polarization state of the probe pulse can be determined, the electric-field amplitude and polarization direction of the THz pulses can be measured.

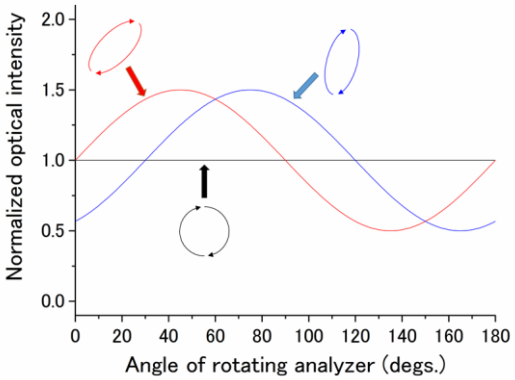

Fig. 5. Normalized optical intensity obtained in rotating-analyzer ellipsometry. The black line shows the case of circularly polarized light. The red and blue lines both represent cases of elliptical polarization, but with different azimuthal angles.

We utilized rotating-analyzer ellipsometry [25] to measure the polarization state of the probe pulses. When rotating the analyzer at the frequency f_1 (20 Hz), the probe pulse was modulated at the frequency $2f_1$ due to the symmetry of the analyzer. Figure 5 shows schematically the normalized optical intensity obtained from general rotating-analyzer ellipsometry. For circularly polarized light (black line), the optical intensity is unity, independent of the rotation angle. On the other hand, for elliptically polarized light (the red and blue lines), the optical intensity oscillates sinusoidally. The amplitude of the oscillation increases with the ellipticity of the probe pulse. According to Eq. (1), this amplitude is proportional to the THz electric-field strength. The difference between two elliptical polarizations (the red and blue lines) corresponds to the azimuthal angle, which appears as a phase shift in the optical-intensity oscillations in rotating-analyzer ellipsometry. Note that the azimuthal angle of the probe pulse has a one-to-one relationship with the orientation of the THz electric field [Eq. (2)]. Therefore, by measuring the amplitude and phase of the oscillation of the optical intensity with rotating-analyzer ellipsometry, we can obtain the amplitude and the orientation of the THz electric field. The optical intensity S_r of the probe pulse, modulated by the THz electric field and the rotating analyzer, is given by

$$S_r = \frac{1}{2}\left(1+\sin A_c \left|E_T\right| \sin\left(2\varphi t - \theta_T\right)\right), \tag{3}$$

where φt is the time-dependent angle of the rotating analyzer.

This type of signal (shown in Fig. 5) can be measured using a lock-in detector. Assuming that $A_c|E_T|<<1$ in Eq. (1), we found the following relationships between the output signals from the lock-in detector and the electric field of a THz pulse:

$$E_{T_x} = \left|E_T\right| \cos\theta_T \propto A_L \sin\phi_L, \tag{4}$$

and

Optics EXPRESS

$$E_{T_y} = |E_T| \sin\theta_T \propto A_L \cos\phi_L . \quad (5)$$

where A_L and ϕ_L are, respectively, the detected amplitude and the phase of the input signal at the lock-in amplifier. Note that $A_L \sin\phi_L$ and $A_L \cos\phi_L$ are typical output signals from a dual-phase lock-in amplifier. Therefore, the *x*-axis and *y*-axis components of the THz electric field can be obtained directly from the outputs of a dual-phase lock-in amplifier.

Normally, PS-THz-TDS has some errors, such as sensitivity differences and non-orthogonality between the measured *x*-axis and *y*-axis components. In our case, imperfections in the ZnTe crystal, the polarization dependence of the beam splitter, and misalignments may have led to such errors. We corrected for these errors by utilizing the dependence of the measured polarization angle upon the actual polarization angle (see Appendix 2).

2.3 Experimental procedure for simultaneous detection

Figure 6 shows a schematic diagram of a PS-THz-TDS optical system expanded to a system for simultaneously measuring the vector waveforms of RCP and LCP THz pulses. We used an optical chopper to eliminate background modulation of the detected signals (explained in detail below).

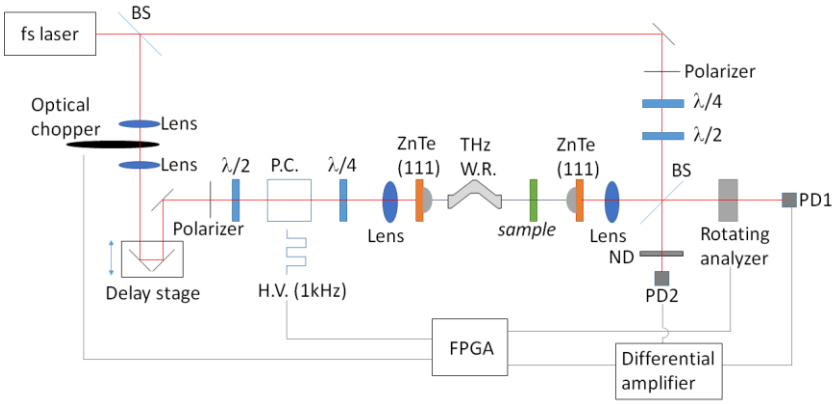

Fig. 6. Schematic overview of a setup for the simultaneous measurement of two-polarization-state THz pulses. W.R. = wave retarder, H.V. = high voltage, P.C. = Pockels cell, BS = beam splitter, ND = neutral-density filter, and PD = photo diode.

Using a field-programmable gate array (FPGA), we integrated an alternating-emission system with the PS-THz-TDS system to measure two-polarization-state THz pulses. The control scheme is similar to a double-modulation scheme [26]. First, we extracted signals synchronized at f_2 (1 kHz) using a relatively short time constant. This process separated the signals from the two polarization states of the THz electric field (see below). Then we carried out lock-in detection at $2f_1$ (40 Hz) to measure the electric-field vector of each polarization state.

Figure 7 shows the timing chart for signal processing related to the separation of the two polarization states of the THz electric field (termed polarizations A and B). Let S_A, S_B, and S_0 be the signal levels of polarization A, polarization B, and the background, respectively, at a given temporal delay. We synchronized the Pockels cell and the optical chopper at 1 kHz; however, their phases were shifted from each other by $\pi/2$. We formed reference signals 1 and 2 so that the information for only one of the polarization states is extracted, and the corresponding background signal is subtracted. By multiplying the acquired data by reference signal 1, we were thus able to extract a signal that originated solely from polarization state A. Similarly, we extracted the data originating from polarization state B by multiplying the acquired data by reference signal 2.

Optics EXPRESS

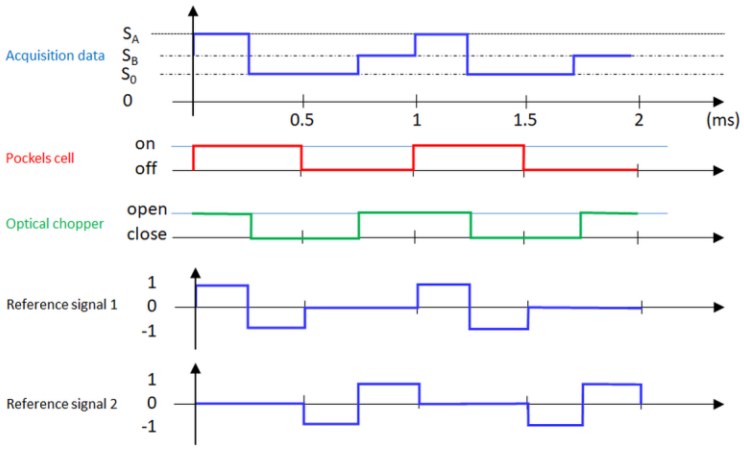

Fig. 7. Timing chart for signal processing.

By sweeping with a delay stage, we acquired the temporal waveforms of the two-polarization-state electric-field vectors at the same time. Figure 8 shows a captured image from the front panel of our measurement software. (In Visualization 1, we show the evolution of the measured temporal waveforms). We measured the temporal waveforms of the RCP and LCP THz pulses simultaneously.

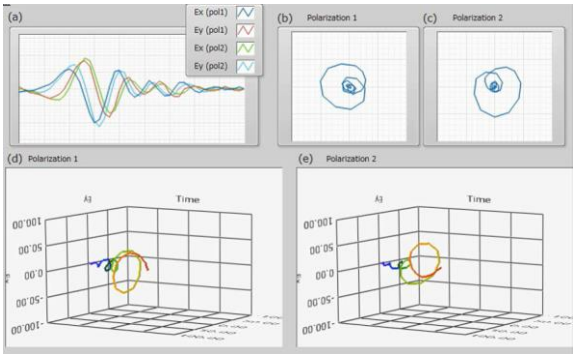

Fig. 8. Captured image from the front panel of our measurement software (see also Visualization 1; × 4 speed playback). (a) Temporal waveforms of the *x*- and *y*-components of two-polarization-state THz pulses. (b) and (c) Projections of the temporal vector waveforms of polarization states 1 and 2 on the *xy*-plane. (d) and (e) Temporal waveforms of the electric-field vectors of polarization states 1 and 2.

3. Measurements of birefringent materials

By using two temporal waveforms of the electric-field vector with different polarization states, we were able to measure the complex refractive indices and sample orientations of birefringent materials. Because the analytical solutions were complicated, we adopted the following technical approach. We assumed angles of the optical axes, and we extracted the two temporal waveforms along these axes from the waveforms of the THz electric-field vectors. Then, from the complex transmittances determined using these waveforms, with and without the sample present, we calculated the refractive indices for each angle and plotted their angular dependences. If the assumed angles were the same as the optical axes of the sample, the refractive index obtained for each polarization should be either n_e or n_o, depending on which polarization component (A or B) corresponds to the extraordinary or ordinary axis (see Appendix 3 for details).

Optics EXPRESS

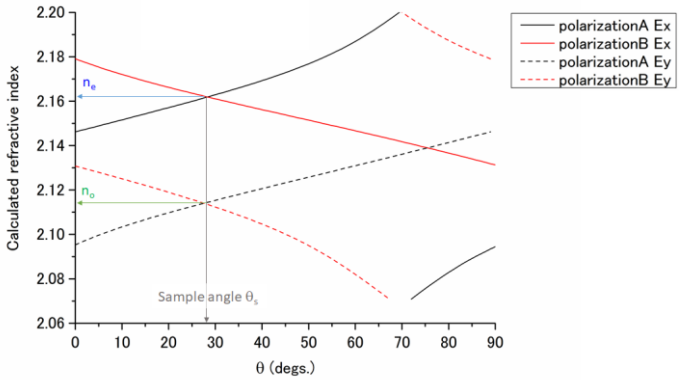

Fig. 9. Determination of the refractive indices and the directions of the slow and fast axes. The measured sample was a quartz disc, and the analyzed frequency was 1.5 THz.

Figure 9 shows the measured result. The measured sample was a 1.5-mm-thick quartz disc, and the analyzed frequency was 1.5 THz. We obtained the sample angle of 28.3 degrees from the crossing points in the graph. At the same time, we obtained the refractive indices n_e = 2.162 and n_o = 2.114.

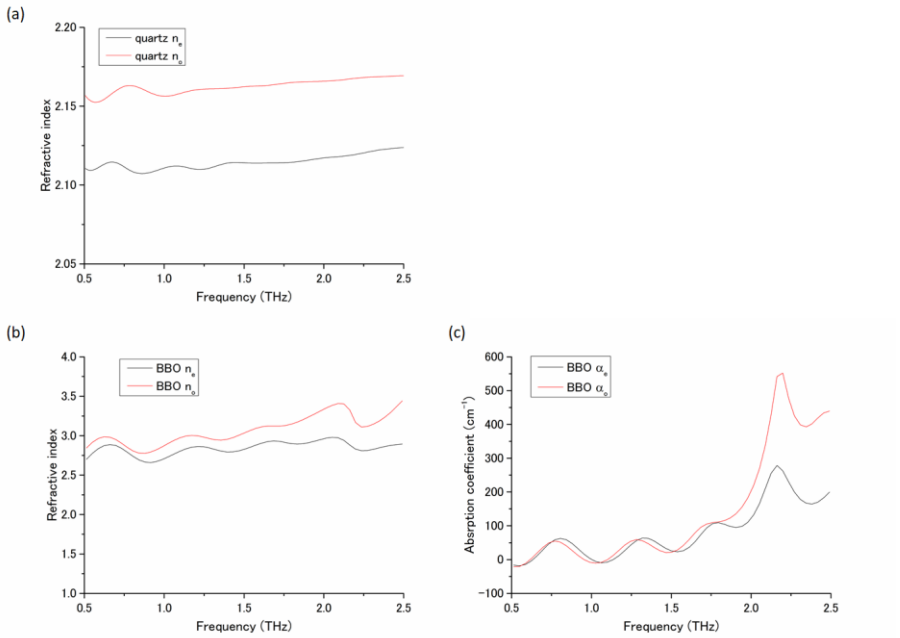

Fig. 10. Measured frequency-dependent refractive indices of (a) quartz and (b) BBO. (c) The absorption coefficient of BBO.

Figure 10 shows the measured spectra of a 1.5-mm-thick quartz disc and a 100-μm-thick barium borate (BBO) crystal. Figure 10(a) shows the measured refractive indices of the quartz disc. We found the refractive index of the fast axis to be 2.11 and that of the slow axis to be 2.16, and they increased slightly with frequency, similar to previously reported results [27]. When we rotated the quartz disc, the difference between the angles of the fast and slow axes and the refractive indices of each axis remained constant, as expected (data not shown). Figure 10(b) shows the real part of the complex refractive index of the BBO crystal and 10(c)

Optics EXPRESS

shows the corresponding absorption coefficient. We observed an absorption peak at 2.2 THz due to a phonon mode [28]. There are also oscillations with a period of 0.5 THz; these correspond to an etalon effect due to Fabry–Pérot oscillations for a sample with a thickness of 100 μm and a refractive index of 3.

4. Conclusion

We demonstrated alternating emission and simultaneous measurements of RCP and LCP THz pulses. We changed the polarization states of the THz pulses periodically by modulating the pump pulses using a Pockels cell. To obtain circularly polarized THz pulses, we used a prismatic THz wave-retarder. We constructed a PS-THz-TDS to measure the vector electric-field waveforms of the THz pulses simultaneously by using a circularly polarized probe pulse and a ZnTe (111) crystal as a THz receiver. Our PS-THz-TDS technique enables the acquisition of orthogonal THz electric-field components directly from the outputs of a dual-phase lock-in amplifier. An FPGA-based controller synchronized the THz emitter and the PS-THz-TDS. We measured eight independent variables (the amplitudes and phases of the two orthogonal components of the RCP and LCP THz pulses) in a single temporal sweep. The reduced measuring time improves the stability of the measurement system. We measured the frequency-dependent complex refractive indices (real and imaginary parts) of the slow and fast axes simultaneously, together with the orientations of the birefringent samples (quartz and BBO) . This technique for emitting and measuring THz pulses with two different polarization states can be expanded to several types of spectroscopic measurements by utilizing information about the polarization-dependence of the materials, such as circular-dichroism spectroscopy and spectroscopic ellipsometry.

Appendix 1. – One-to-one relationship between the THz electric-field vector and the polarization state of the probe pulse

We calculated the THz-induced birefringence of a ZnTe (111) crystal by using the equations in [24]. The propagation direction of the probe pulse and the THz pulse are given by the unit vector $\hat{\mathbf{s}} = 1/3(1,1,1)$. We calculated the changes in the refractive indices from Eqs. (20) and (21) of [24], obtaining

$$\Delta n_1 = -\frac{\chi^{(2)}}{2\sqrt{\varepsilon_r}}\left(-\sqrt{\frac{2}{3}\left(E'_{T_y}{}^2 + E'_{T_z}{}^2\right)}\right), \tag{6}$$

and

$$\Delta n_2 = -\frac{\chi^{(2)}}{2\sqrt{\varepsilon_r}}\left(\sqrt{\frac{2}{3}\left(E'_{T_y}{}^2 + E'_{T_z}{}^2\right)}\right), \tag{7}$$

where $\chi^{(2)}$ and ε_r are the second-order susceptibility and the relative permitivity of the ZnTe crystal, and E'_{T_x} and E'_{T_y} are the THz electric fields in the (111) plane. The refractive index difference is thus given by

$$\Delta n \equiv (\Delta n_1 - \Delta n_2) = \sqrt{\frac{2}{3}}\frac{\chi^{(2)}}{\sqrt{\varepsilon_r}}\left|E'_T\right|. \tag{8}$$

As Eq. (8) shows, Δn depends only on the strength of the THz electric-field (and does not depend on its direction).

Next, we calculated the polarization direction of the first propagation mode of the THz-induced birefringence $\mathbf{E}'_{01}$ (Eq. (24) of [24]), obtaining

Optics EXPRESS

$$\mathbf{E'_{01}} = \begin{pmatrix} 0 \\ \frac{\sqrt{6}}{3} E'_{T_y} \\ -\frac{\sqrt{6}}{3}\left(\sqrt{E'^{\,2}_{T_y} + E'^{\,2}_{T_z}} + E'_{T_z}\right) \end{pmatrix}. \tag{9}$$

The orientation of the main axis of the THz-induced birefringence is given by

$$\begin{aligned} &\arctan \frac{E'_{01y}}{E'_{01z}} \\ &= \arctan \frac{\frac{\sqrt{6}}{3} E'_{T_y}}{-\frac{\sqrt{6}}{3}\left(\sqrt{E'^{\,2}_{T_y} + E'^{\,2}_{T_z}} + E'_{T_z}\right)} \\ &= \arctan \frac{-|E'_T| \sin\theta_T}{|E'_T| + |E'_T| \cos\theta_T} \\ &= -\frac{\theta_T}{2}. \end{aligned} \tag{10}$$

Contrary to the refractive-index difference, the orientation of the main axis depends only on the direction of the THz electric field (and does not depend on the field strength). Using Eqs. (8) and (10), we obtained Eqs. (1) and (2) for the case of probing with a circularly polarized probe pulse.

Appendix 2. - Calibration of the electric-field vector

Using the optical system shown in Fig. 11(a), we measured the temporal waveforms of the THz electric-field vector with the PS-THz-TDS while rotating the W.G. polarizer in steps of 22.5° from –90° to 90°. Fig. 11(b) shows examples of the measured temporal waveforms. From these results, in Fig. 12 we plotted the dependence of the measured polarization angles before adopting the calibration technique in Fig. 12. The measured polarization angle is defined as the direction in which the electric-field intensity of the THz temporal waveform is a maximum. We measured each temporal waveform six times, and all the measurements almost overlapped at each angle, as shown in Fig. 12. The actual orientation θ_T of the THz electric field and the measured polarization angle θ_{Tex} have the following relationship:

$$\tan\theta_T = \alpha \frac{\sin\left(\theta_{Tex} - \Delta\theta_y\right)}{\cos\left(\theta_{Tex} - \Delta\theta_x\right)}, \tag{11}$$

where α is the ratio of the sensitivity difference between the *x*-axis and *y*-axis components, and $\Delta\theta_x$ and $\Delta\theta_y$ are the differences of the measured angles from the base coordinates of the optical system. The degree of non-orthogonality is reflected in the difference $\Delta\theta_y$ - $\Delta\theta_x$. Using Eq. (11), we fitted the plotted data in Fig. 12 (the red line) and obtained the calibration parameters α = 0.877, $\Delta\theta_x$ = 2.68°, and $\Delta\theta_y$ = 7.96°. We used these calibration parameters throughout this paper. By adopting our calibration technique, we could obtain a linear relationship between the actual orientation θ_T of the THz electric field and the measured polarization angle θ_{Tex}. A significant feature of this calibration technique is that it uses only the direction of oscillation of the THz pulses (and does not depend on the power of the THz pulse). Thus, we avoid the influence of temporal fluctuations in the laser power. In addition,

Optics EXPRESS

using this technique, we can separate the three factors α, $\Delta\theta_x$, and $\Delta\theta_y$, which are usually difficult to disentangle.

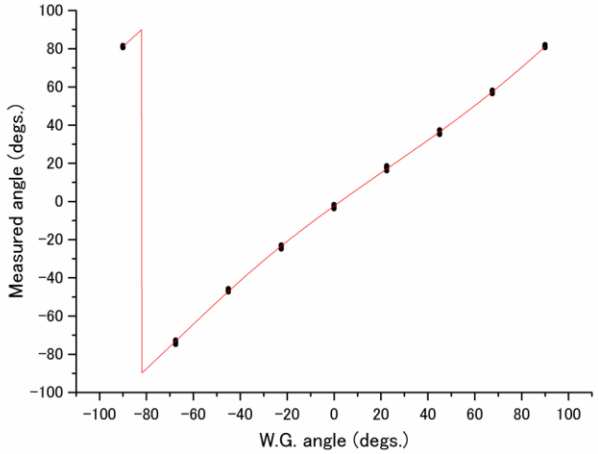

Fig. 11. (a) Schematic overview of the setup for measuring the calibration parameters. (b) Measured temporal waveforms of the electric-field vector at each angle of the wire-grid (W.G.) polarizer.

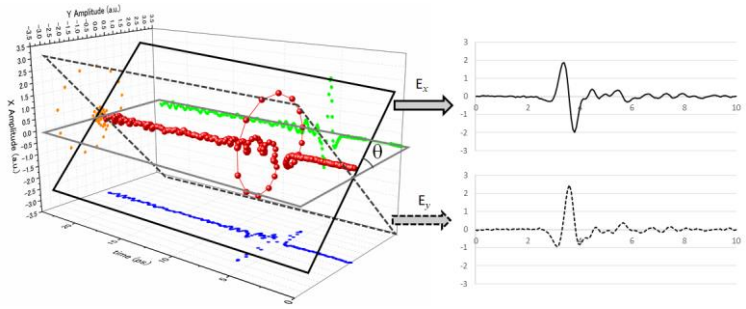

Fig. 12. Dependence of the measured polarization angle on the angle of the W.G. polarizer before calibration. Six measurement results overlap at each data point. The red line shows a fit to the data using Eq. (11).

Appendix 3. – Determination of refractive indices and the directions of the slow and fast axes

The electric field of the initial THz pulses (without a sample present) of one polarization state can be represented by a Jones vector as follows:

$$\mathbf{E}_{\mathrm{ref}} = \begin{bmatrix} E_{x0}e^{i\phi_{x0}} \\ E_{y0}e^{i\phi_{y0}} \end{bmatrix}. \tag{12}$$

Assuming that the circular birefringence, circular dichroism, and magnetism of the sample can be neglected, the electric field of a THz pulse after passing through the sample can be represented by

$$\mathbf{E} = \begin{bmatrix} (T_{\mathrm{a}}e^{i\phi_{\mathrm{a}}}\cos^2\theta_{\mathrm{s}} + T_{\mathrm{b}}e^{i\phi_{\mathrm{b}}}\sin^2\theta_{\mathrm{s}})E_{x0}e^{i\phi_{x0}} + (T_{\mathrm{a}}e^{i\phi_{\mathrm{a}}} - T_{\mathrm{b}}e^{i\phi_{\mathrm{b}}})E_{y0}e^{i\phi_{y0}}\sin\theta_{\mathrm{s}}\cos\theta_{\mathrm{s}} \\ (T_{\mathrm{a}}e^{i\phi_{\mathrm{a}}} - T_{\mathrm{b}}e^{i\phi_{\mathrm{b}}})E_{x0}e^{i\phi_{x0}}\sin\theta_{\mathrm{s}}\cos\theta_{\mathrm{s}} + (T_{\mathrm{a}}e^{i\phi_{\mathrm{a}}}\cos^2\theta_{\mathrm{s}} + T_{\mathrm{b}}e^{i\phi_{\mathrm{b}}}\sin^2\theta_{\mathrm{s}})E_{y0}e^{i\phi_{y0}} \end{bmatrix}, \tag{13}$$

Optics EXPRESS

where E_{x0} and E_{y0} are the *x*- and *y*-components of the electric-field amplitudes, and ϕ_{x0} and ϕ_{y0} are the phases of the *x*- and *y*-components of the initial electric field. The quantities $T_a e^{i\phi_a}$ and $T_b e^{i\phi_b}$ are the transmittance and phase shift due to transmission through a birefringent sample for each orthogonal axis (the slow and fast axes); they can be translated into the complex refractive indices of the slow and fast axes for a sample of known thickness. The quantity θ_s is the sample orientation angle. In Eq. (13), each row includes both $T_a e^{i\phi_a}$ and $T_b e^{i\phi_b}$. However, to multiply a rotation matrix by the sample angle θ_s, we convert Eqs. (12) and Eq. (13) into the following forms:

$$\mathbf{E}_{\mathrm{ref}\theta_s} = \begin{bmatrix} E_{x0}e^{i\phi_{x0}}\cos\theta_s + E_{y0}e^{i\phi_{y0}}\sin\theta_s \\ -E_{x0}e^{i\phi_{x0}}\sin\theta_s + E_{y0}e^{i\phi_{y0}}\cos\theta_s \end{bmatrix}, \tag{14}$$

$$\mathbf{E}_{\theta_s} = \begin{bmatrix} T_a e^{i\phi_a}(E_{x0}e^{i\phi_{x0}}\cos\theta_s + E_{y0}e^{i\phi_{y0}}\sin\theta_s) \\ T_b e^{i\phi_b}(-E_{x0}e^{i\phi_{x0}}\sin\theta_s + E_{y0}e^{i\phi_{y0}}\cos\theta_s) \end{bmatrix}. \tag{15}$$

In Eq. (15), each row includes only $T_a e^{i\phi_a}$ or $T_b e^{i\phi_b}$. Thus, if we can determine the angle of the optical axis of the sample, we can calculate the complex refractive indices of the slow and fast axes independently using Eqs. (14) and (15). In addition, this calculation is not influenced by the initial polarization state of the THz pulse [Eq. (14)], because the information about the initial pulse is eliminated by dividing Eq. (15) by Eq. (14) in this procedure. This means that the same refractive indices are obtained from calculations using the temporal waveforms of THz pulses with two different polarization states at the correct sample angle.

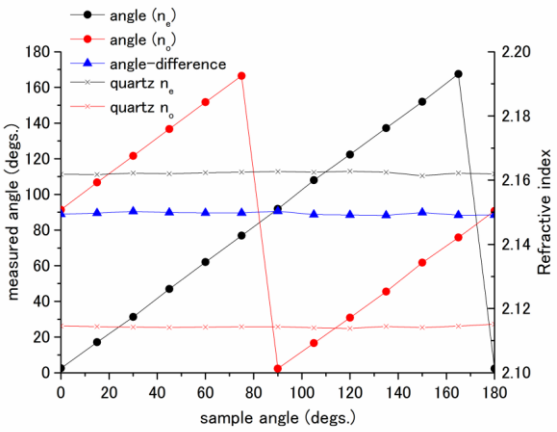

Fig. 13. Extraction of temporal waveforms at an angle θ from the temporal waveform of the THz electric-field vector.

Using the measured temporal waveforms of the electric-field vector of the THz pulses with and without the sample, we searched for the correct sample angle by the following procedure: First, we assumed the angles of the optical axes and extracted two temporal waveforms along them from the waveforms of the THz electric-field vectors (Fig. 13). Then, from the complex transmittances determined using these waveforms with and without the sample present, we calculated the refractive indices for each angle, and plotted their angle dependence (Fig. 9). If the assumed angles are the same as the optical axes of the sample, the refractive index obtained for each polarization is either n_e or n_o, depending on which polarization component (A or B) corresponds to the extraordinary or ordinary axis. The

Optics EXPRESS

calculated curves for the refractive indices for polarizations A and B, therefore, should coincide with each other in this case. By finding the crossing points from the graph, we can obtain the correct sample angle and refractive indices, as can be seen in Fig. 9. Note that this procedure can be performed for each frequency component.

In this manner, we can obtain both the frequency-dependent refractive indices and the sample orientation angle; however, the sample angle must be the same at each frequency. We thus calculated an average value of the sample orientation angle to increase the accuracy. Here, we used the values of the sample orientation angle so-obtained only in frequency regions with high signal-to-noise ratios in order to avoid decreasing the accuracy of the measurement, especially in low signal-to-noise frequency regions, such as at the peak absorption frequency.

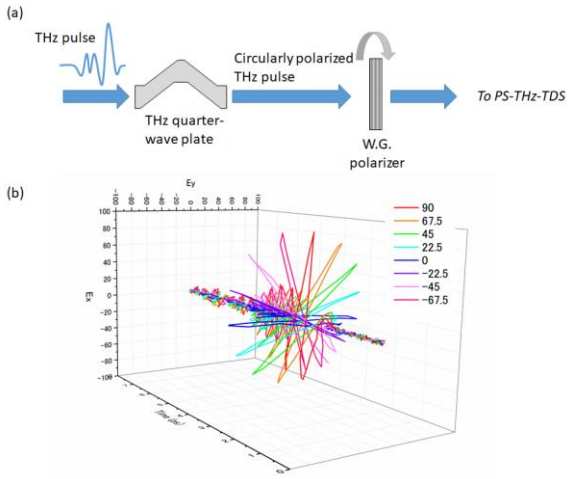

Fig. 14. Measured refractive indices and the orientations of the slow and fast axes with a rotating quartz disc. The angle difference between the slow and fast axes is also plotted.

To use the circularly polarized THz pulses, both the slow and the fast axes of a sample contribute equally to the signal. Therefore, the dependence of the precision on the sample angle can be minimized by using circularly polarized THz pulses. For this purpose, the quality of the polarization states of the RCP and LCP THz pulses is important. Normalized Stokes parameters (S_0=1.0) were S_1=0.01442, S_2=-0.03268, S_3=-0.9994 for polarization A and S_1=-0.10760, S_2=0.04886, S_3=0.9929 for polarization B at 1.5 THz. To confirm dependence of the precision on the sample angle, we measured the refractive indices and the orientations of the slow and fast axes by rotating a quartz disc step by step. We carried out measurement while rotating the quartz disc in steps of 15° from 0° to 180°. Figure 14 shows the measured angle of the fast and slow axes and each refractive index at 1.5 THz. The measured angle of the fast axis (black line with filled circles) and slow axis (red line with filled circles) changed linearly as the quartz disc was rotated. The difference between the angles of the fast and slow axes (blue line with filled triangles) and the refractive indices of each axis were constant as the sample was rotated. If we use the data before calibration, the measured angles do not change linearly (data not shown). In this manner, we could measure the frequency-dependent complex refractive indices (real and imaginary parts) and the orientations of the slow and fast axes of birefringent materials precisely with any sample direction, except for statistical uncertainty.

Acknowledgments

Y.K. and H.T. thank A. Hiruma, K. Yamamoto, and T. Hara for their encouragement. The authors thank H. Satozono and T. Yasuda for fruitful discussions about this research. The

Optics EXPRESS

authors also thank S. Oishi and S. Yamagishi for technical support in preparing the Pockels cell.

References

1. T. Nagashima and M. Hangyo, "Measurement of complex optical constants of a highly doped Si wafer using terahertz ellipsometry," Appl. Phys. Lett. **79**(24), 3917–3919 (2001).
2. J. Xu, J. Galan, G. Ramian, P. Savvidis, A. Scopatz, R. R. Birge, S. J. Allen, and K. Plaxco, "Terahertz circular dichroism spectroscopy of biomolecules," Proc. SPIE **5268**, 19–26 (2004).
3. M. Okano and S. Watanabe, "Anisotropic optical response of optically opaque elastomers with conductive fillers as revealed by terahertz polarization spectroscopy," Sci. Rep. **6**(1), 39079 (2016).
4. I. Kézsmárki, N. Kida, H. Murakawa, S. Bordács, Y. Onose, and Y. Tokura, "Enhanced directional dichroism of terahertz light in resonance with magnetic excitations of the multiferroic $Ba_2CoGe_2O_7$ oxide compound," Phys. Rev. Lett. **106**(5), 057403 (2011).
5. J. N. Heyman, D. Bell, and T. Khumalo, "Terahertz photo-Hall measurements of carrier mobility in GaAs and InP," Appl. Phys. Lett. **88**(16), 162104 (2006).
6. X. Li, M. Bamba, Q. Zhang, S. Fallahi, G. C. Gardner, W. Gao, M. Lou, K. Yoshioka, M. J. Manfra, and J. Kono, "Vacuum Bloch-Siegert shift in Landau polaritons with ultra-high cooperativity," Nat. Photonics **12**(6), 324–329 (2018).
7. N. Yasumatsu and S. Watanabe, "Precise real-time polarization measurement of terahertz electromagnetic waves by a spinning electro-optic sensor," Rev. Sci. Instrum. **83**(2), 023104 (2012).
8. N. Yasumatsu, A. Kasatani, K. Oguchi, and S. Watanabe, "High-speed terahertz time-domain polarimeter based on an electro-optic modulation technique," Appl. Phys. Express **7**(9), 092401 (2014).
9. N. Nemoto, T. Higuchi, N. Kanda, K. Konishi, and M. Kuwata-Gonokami, "Highly precise and accurate terahertz polarization measurements based on electro-optic sampling with polarization modulation of probe pulses," Opt. Express **22**(15), 17915–17929 (2014).
10. E. Castro-Camus, J. Lloyd-Hughes, M. B. Johnston, M. D. Fraser, H. H. Tan, and C. Jagadish, "Polarization-sensitive terahertz detection by multicontact photoconductive receivers," Appl. Phys. Lett. **86**(25), 254102 (2005).
11. H. Makabe, Y. Hirota, M. Tani, and M. Hangyo, "Polarization state measurement of terahertz electromagnetic radiation by three-contact photoconductive antenna," Opt. Express **15**(18), 11650–11657 (2007).
12. O. Arteaga and A. Canillas, "Analytic inversion of the Mueller-Jones polarization matrices for homogeneous media," Opt. Lett. **35**(4), 559–561 (2010).
13. X.-C. Zhang, X. F. Ma, Y. Jin, T. M. Lu, E. P. Boden, P. D. Phelps, K. R. Stewart, and C. P. Yakymyshyn, "Terahertz optical rectification from a nonlinear organic crystal," Appl. Phys. Lett. **61**(26), 3080–3082 (1992).
14. E. Estacio, S. Saito, T. Nakazato, Y. Furukawa, N. Sarukura, M. Cadatal, M. H. Pham, C. Ponseca, Jr., H. Mizuseki, and Y. Kawazoe, "Birefringence of β-BaB2O4 crystal in the terahertz region for parametric device design," Appl. Phys. Lett. **92**(9), 091116 (2008).
15. K. Song, Z. Tian, W. Zhang, and M. Wang, "Temperature-dependent birefringence of lithium triborate, LBO in the THz regime," Sci. Rep. **7**(1), 8122 (2017).
16. H. Hoshina, S. Ishii, S. Yamamoto, Y. Morisawa, H. Sato, T. Uchiyama, Y. Ozaki, and C. Otani, "Terahertz spectroscopy in polymer research: assignment of intermolecular vibrational modes and structural characterization of poly (3-hydroxybutyrate," IEEE Trans. THz Sci. Technol. **3**(3), 248–258 (2013).
17. S. Katletz, M. Pfleger, H. Pühringer, M. Mikulics, N. Vieweg, O. Peters, B. Scherger, M. Scheller, M. Koch, and K. Wiesauer, "Polarization sensitive terahertz imaging: detection of birefringence and optical axis," Opt. Express **20**(21), 23025–23035 (2012).
18. C. Jördens, M. Scheller, M. Wichmann, M. Mikulics, K. Wiesauer, and M. Koch, "Terahertz birefringence for orientation analysis," Appl. Opt. **48**(11), 2037–2044 (2009).
19. A. J. Danner, T. Tyc, and U. Leonhardt, "Controlling birefringence in dielectrics," Nat. Photonics **5**(6), 357–359 (2011).
20. K. A. Niessen, M. Xu, and A. G. Markelz, "Terahertz optical measurements of correlated motions with possible allosteric function," Biophys. Rev. **7**(2), 201–216 (2015).
21. Q. Chen, M. Tani, Z. Jiang, and X.-C. Zhang, "Electro-optic transceivers for terahertz-wave applications," J. Opt. Soc. Am. B **18**(6), 823–831 (2001).
22. Y. Kawada, T. Yasuda, A. Nakanishi, K. Akiyama, K. Hakamata, and H. Takahashi, "Achromatic prism-type wave plate for broadband terahertz pulses," Opt. Lett. **39**(9), 2794–2797 (2014).
23. N. C. J. van der Valk, W. A. M. van der Marel, and P. C. M. Planken, "Terahertz polarization imaging," Opt. Lett. **30**(20), 2802–2804 (2005).
24. N. C. J. van der Valk, T. Wenckebach, and P. C. M. Planken, "Full mathematical description of electro-optic detection in optically isotropic crystals," J. Opt. Soc. Am. B **21**(3), 622–631 (2004).
25. D. E. Aspnes and A. A. Studna, "High precision scanning ellipsometer," Appl. Opt. **14**(1), 220–228 (1975).
26. S. P. Mickan, K.-S. Lee, T.-M. Lu, J. Munch, D. Abbott, and X.-C. Zhang, "Double modulated differential THz-TDS for thin film dielectric characterization," Microelectronics J. **33**(12), 1033–1042 (2002).
27. E. E. Russell and E. E. Bell, "Measurement of the optical constants of crystal quartz in the far infrared with the asymmetric Fourier-transform method," J. Opt. Soc. Am. **57**(3), 341–348 (1967).

Optics EXPRESS

28. J. Liu, X. Guo, J. Dai, and X.-C. Zhang, "Optical property of beta barium borate in terahertz region," Appl. Phys. Lett. **93**(17), 171102 (2008).